Electronic Supplementary Material (ESI) for ChemComm.

Electronic Supplementary Information for

Electronic structure modulation of Mo sites in anion and cation co-doped MoO_2 nanospheres for electrocatalytic water oxidation

Chunyan Zhang, ‡ Ling Wang, ‡ Zhuwei Cao, Rui Li, Sheng Ye*

School of Materials and Chemistry & School of Plant Protection, Anhui Agricultural University, Hefei 230036, China

***Corresponding author**

E-mail: sye503@ahau.edu.cn

‡ These authors contributed equally to this work: Chunyan Zhang and Ling Wang.

Experimental

Material

$(NH_4)_6Mo_7O_{24}\cdot 4H_2O$ was purchased from Sinopharm Chemical Reagent Co., Ltd. Both $NaBH_4$ and HCl were from Macklin Co., Ltd. $Ni(NO_3)_2\cdot 6H_2O$ was provided by Aladdin Co., Ltd. The water used in the experiments was purified by a Millipore system. All purchased reagents can be used directly without further purification.

Synthesis of MoO_2 nanospheres

Firstly, MoO_2 were synthesized by hydrothermal method. Specifically, slowly drop aqueous solution with 15 mmol sodium borohydride dissolved in 50 ml distilled water into a solution containing 1 mmol of ammonium molybdate and 300 ml of distilled water under magnetic stirring. After 10 min, the pH value of above solution was adjusted to 5 by using concentrated 37% HCl. And the mixed solution was strongly stirred at room temperature for 3 h. The brown black solution was transferred to a 500 mL polytetrafluoroethylene lined autoclave and held at 220 ºC for 20 h. After centrifugation, the resulted samples were obtained by washing with 95% ethanol and drying at room temperature.

Synthesis of Ni-MoO_2, N-MoO_2 and Ni/N-MoO_2 nanospheres

The synthesis methods of the three kinds of samples were similar to those of MoO_2. Ni-MoO_2 was prepared by adding 2 wt % $Ni(NO_3)_2\cdot 6H_2O$ in the preparation process. For comparison, samples were fabricated by the same procedure with different percentages of $Ni(NO_3)_2\cdot 6H_2O$. While N-MoO_2 and Ni/N-MoO_2 composites were synthesized by calcining the bulk MoO_2 and Ni-MoO_2 composites respectively at 450 ºC for 30 min

and 150 min under NH_3 atmosphere at a heating speed of 2 ºC min^{-1}. For comparison, samples were fabricated by the same procedure with different calcining time.

Characterizations

Field emission scanning electron microscope (SEM, Hitachi S4800) and transmission electron microscope (TEM, Tecnai G2 F20) were used to characterize the morphology and structural information of the prepared samples. The high-resolution transmission electron microscope (HRTEM, JEM-2100 plus) image was tested on the transmission electron microscope. Fourier transform infrared spectroscopy (FTIR, Nicolet iS 10) was recorded on the Brooke tensor II Fourier transform infrared spectrometer. The powder X-ray diffraction (XRD, X' Pert PRO MPD) analysis of the composite was carried out using Rigaku D/Max 2500 PC diffractometer (test range: 10-80 °, working voltage: 40 V, working current: 20 mA). Thermo Science 250Xi system was used for X-ray photoelectron spectroscopy (XPS, Thermo Kalpha) measurement with monochromatic Al Kα as the excitation source, the binding energy was calibrated with reference to the C1S peak of 284.8 eV.

Electrochemical measurements

In 1.0 M KOH electrolyte, all electrochemical measurements of OER activity of the prepared materials were performed using an electrochemical workstation (CHI 760E, CH Instruments Ins., Shanghai, China). Using the standard three electrode system, prepared the catalyst into a 2 mg mL^{-1} solution, in which the volume ratio of water, ethanol and 5 wt% Nafion solution is 8:1:1. Then, dripped it to foam nickel (0.5×0.5 cm^2) as the working electrode, silver/silver chloride electrode as the reference electrode,

and platinum plate as the counter electrode. The relationship between all measured potentials and the reversible hydrogen electrode (RHE) is reported according to the following equation: $E_{(RHE)} = E_{(AgCl/Ag)} + (0.24+ 0.059\ pH)$ V.

In 1.0 M KOH electrolyte solution, all linear sweep voltammetry curves (LSV) were measured at a scanning rate of 5 mV s^{-1} within the RHE range of 0.1-0.3 V. According to the formula (η= a + blog (abs (j))) to calculate the Tafel curve (b: Tafel slope, j: current density). The electrochemical impedance spectroscopy (EIS) measurement was carried out under the condition that RHE was 1.57 V, frequency was from 0.1 Hz to 1 $\times 10^6$ Hz. The closed cycle voltammetry (CV) curves at different scanning rates were measured to study the double-layer capacitance (C_{dl}).

DFT calculations

The DFT results were obtained plane wave basis sets, periodic boundary conditions of CASTEP. The configurations of the systems were optimized by fully relaxing the atomic structures until the remaining forces were less than 0.01 eV/Å. A cutoff energy of 600 eV was used for the GGA-PBE and plane wave basis in all relaxation processes. For self-consistent field (SCF) calculations, the convergence criteria for total energy and electron density were set to 1×10^{-6} au. To model the (-111) plane of MoO_2. To match the lattice parameters. To avoid interactions with neighboring atomic layers, a vacuum region of 15 Å was set along the z direction, which had no effect on the total energy. The Brillouin zone sampling was set to 2×2×1 k-points. During the optimization of the configurations, the atomic structures were fully relaxed until the remaining forces were less than 0.01 eV/Å. To improve accuracy. According to the

literature description, the absorption energy of the free energy change (ΔGH) was calculated and used to observe catalytic activity.

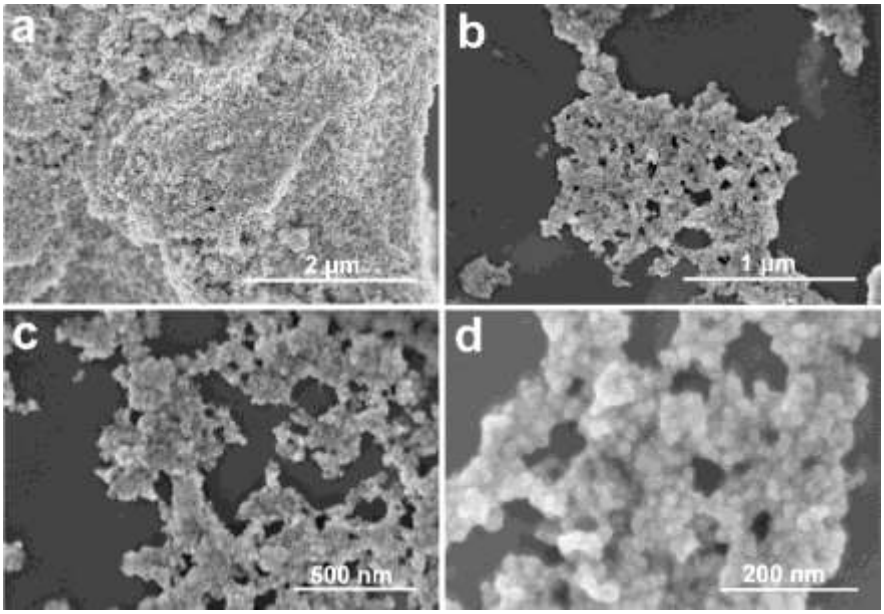

Fig. S1 SEM images of MoO_2.

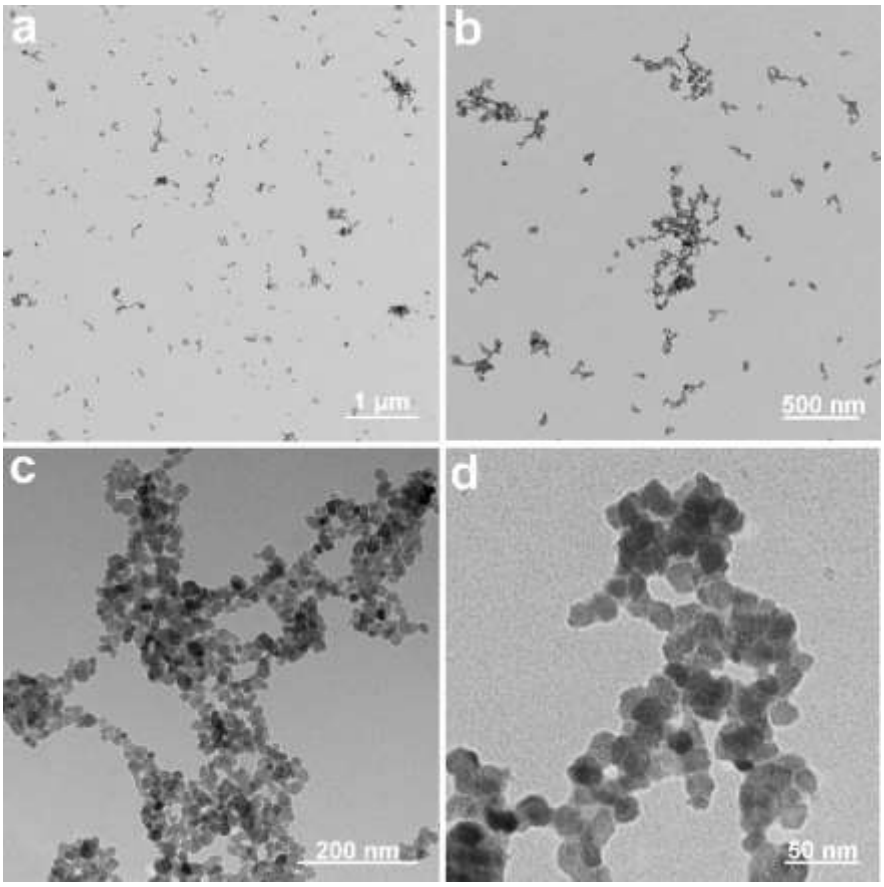

Fig. S2 TEM images of MoO_2.

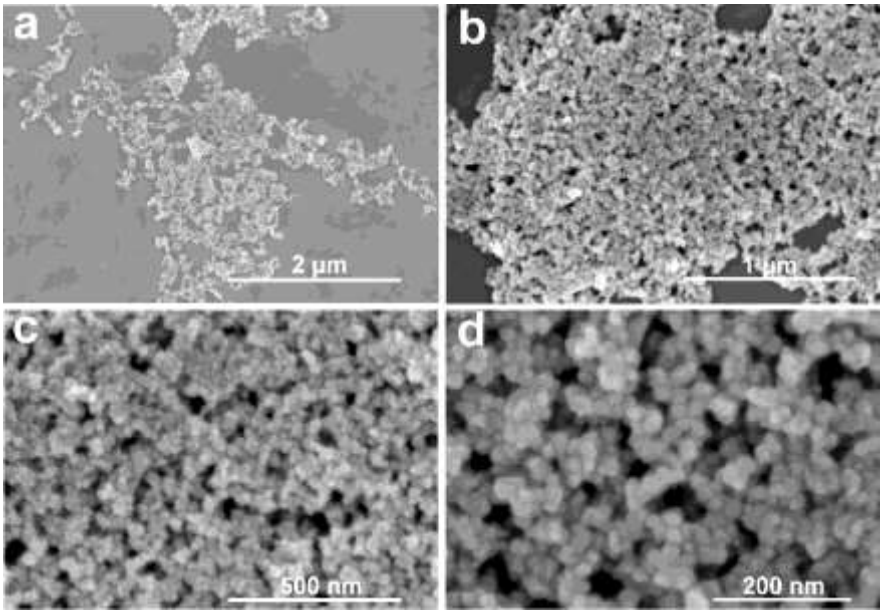

Fig. S3 SEM images of Ni-MoO_2.

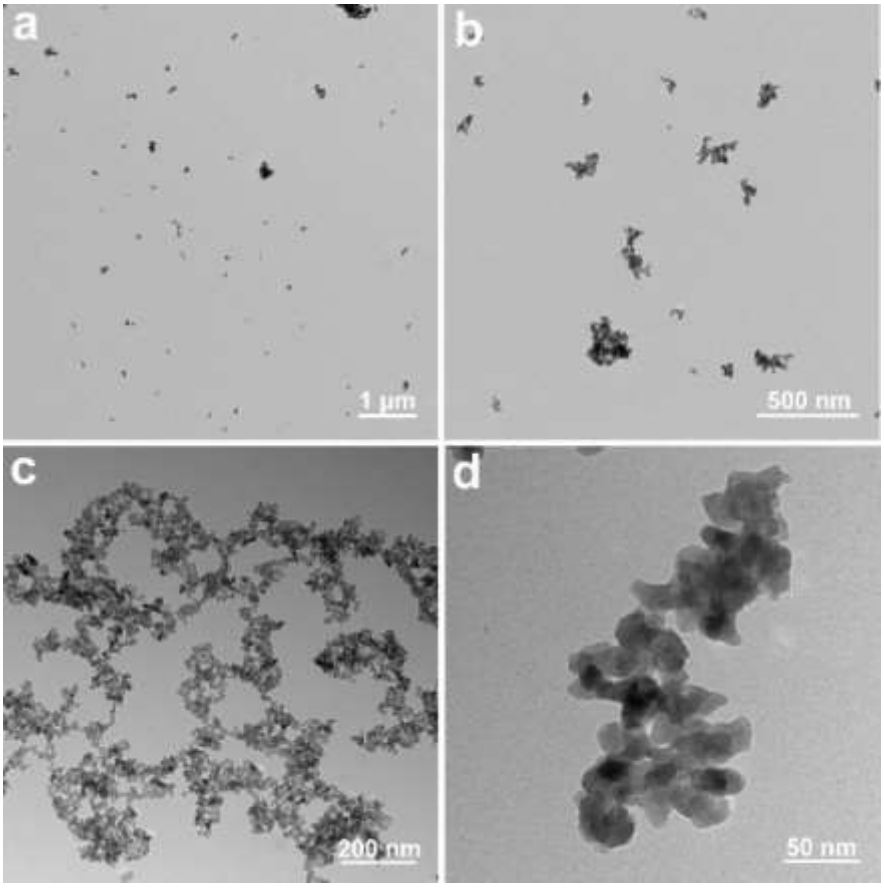

Fig. S4 TEM images of Ni-MoO_2.

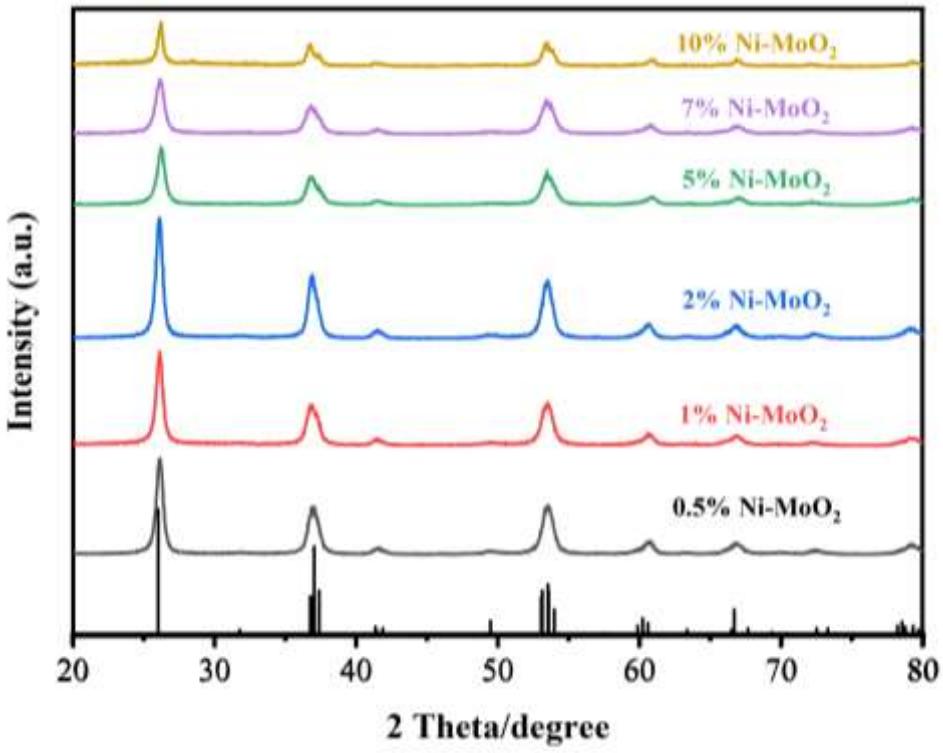

Fig. S5 XRD patterns of the as-prepared Ni-MoO_2 catalysts with different configurations.

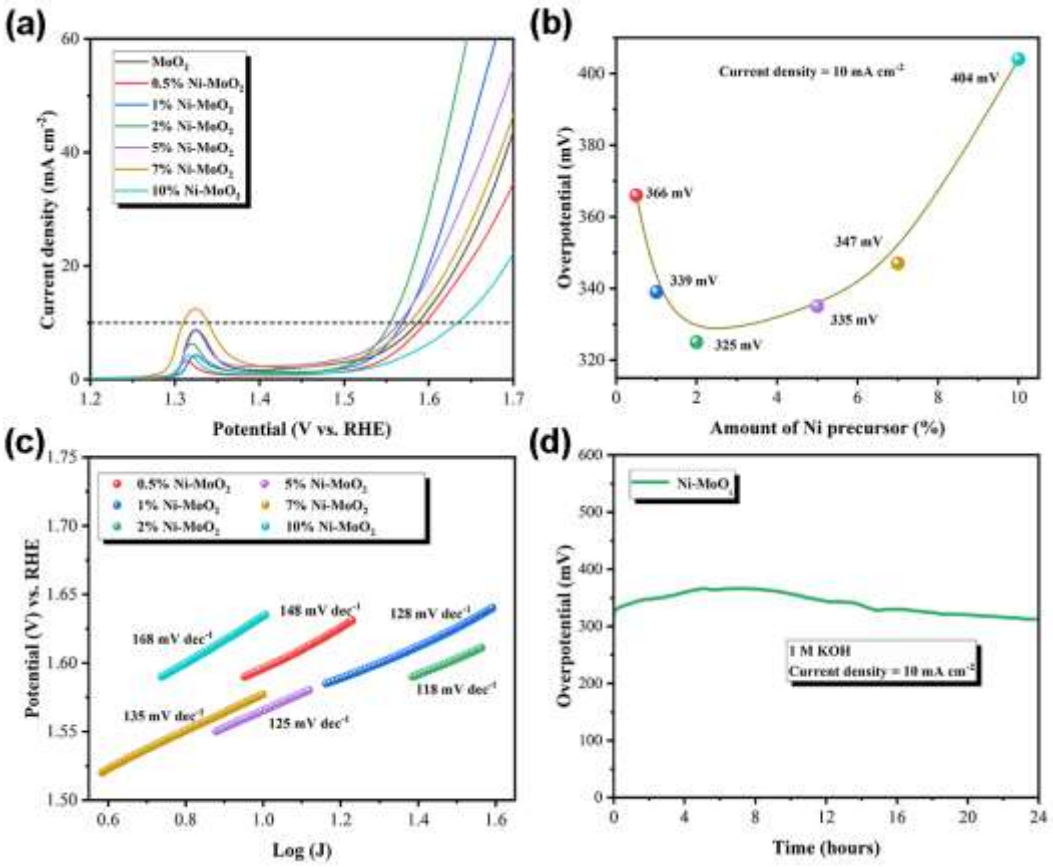

Fig. S6 (a) Polarization curves. (b) Overpotential comparison diagram at 10 mA cm^{-2}. (c) Tafel slopes of the as-prepared Ni-MoO_2 catalysts with different configurations. (d) Chronopotentiometric responses of Ni-MoO_2 at the current density of 10 mA cm^{-2}.

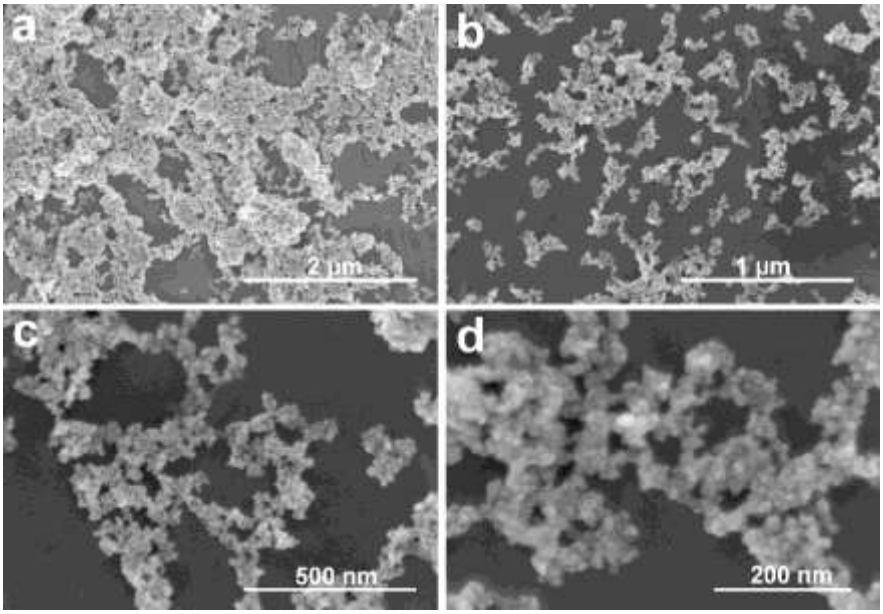

Fig. S7 SEM images of N-MoO_2.

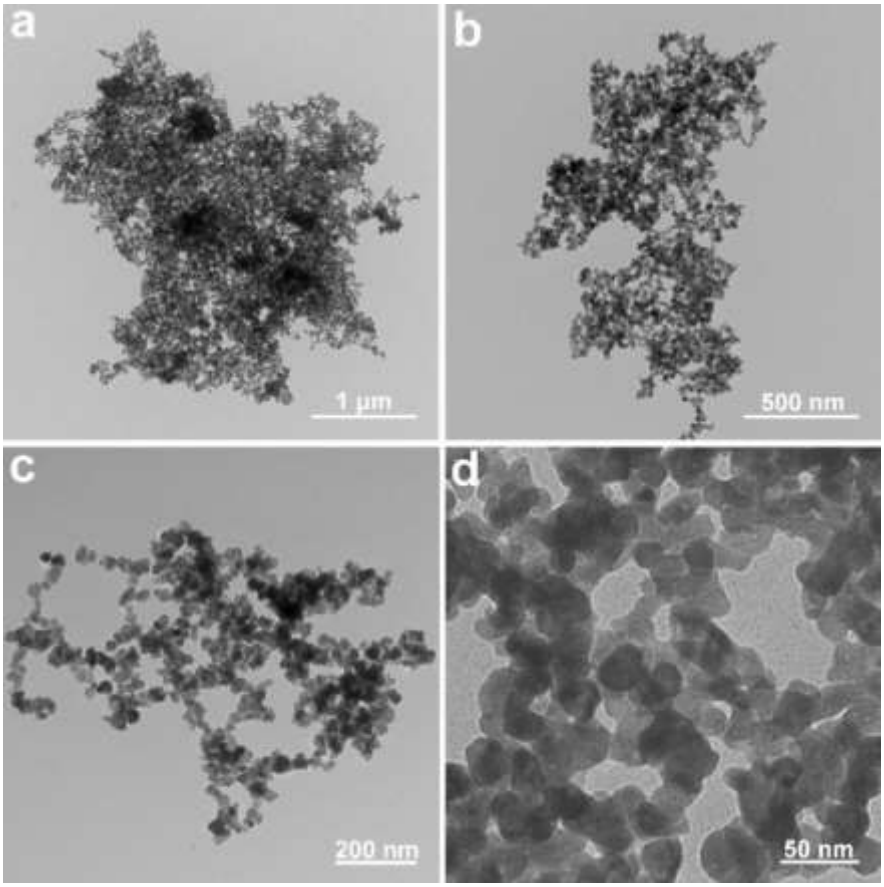

Fig. S8 TEM images of N-MoO_2.

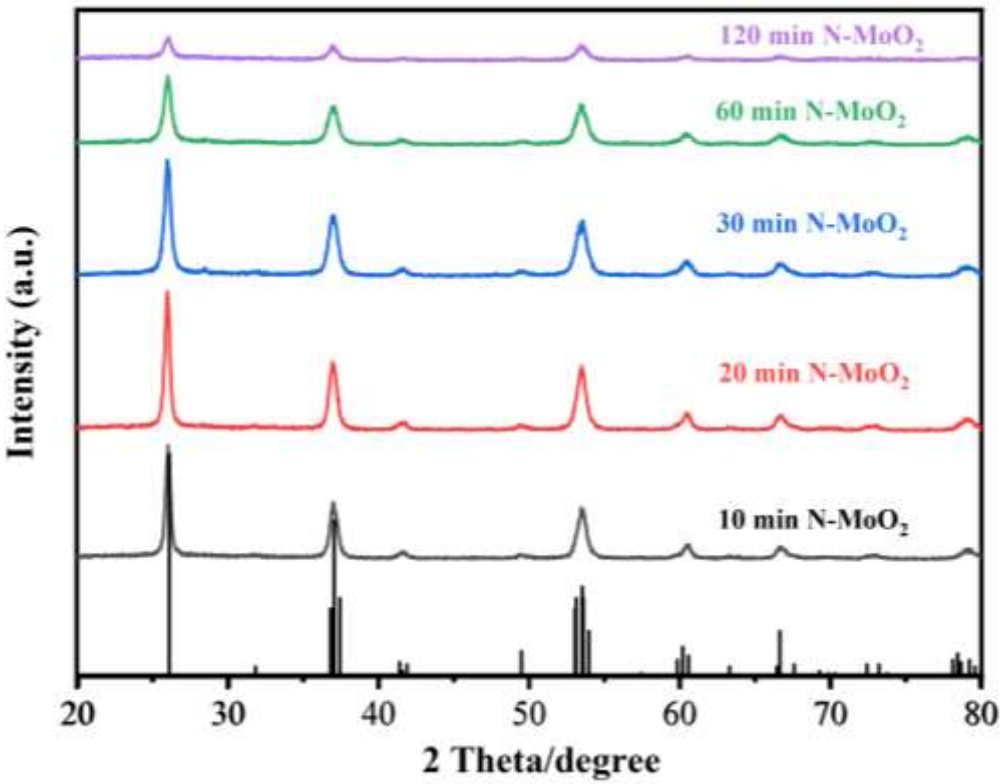

Fig. S9 XRD patterns of the as-prepared N-MoO_2 catalysts with different calcination times.

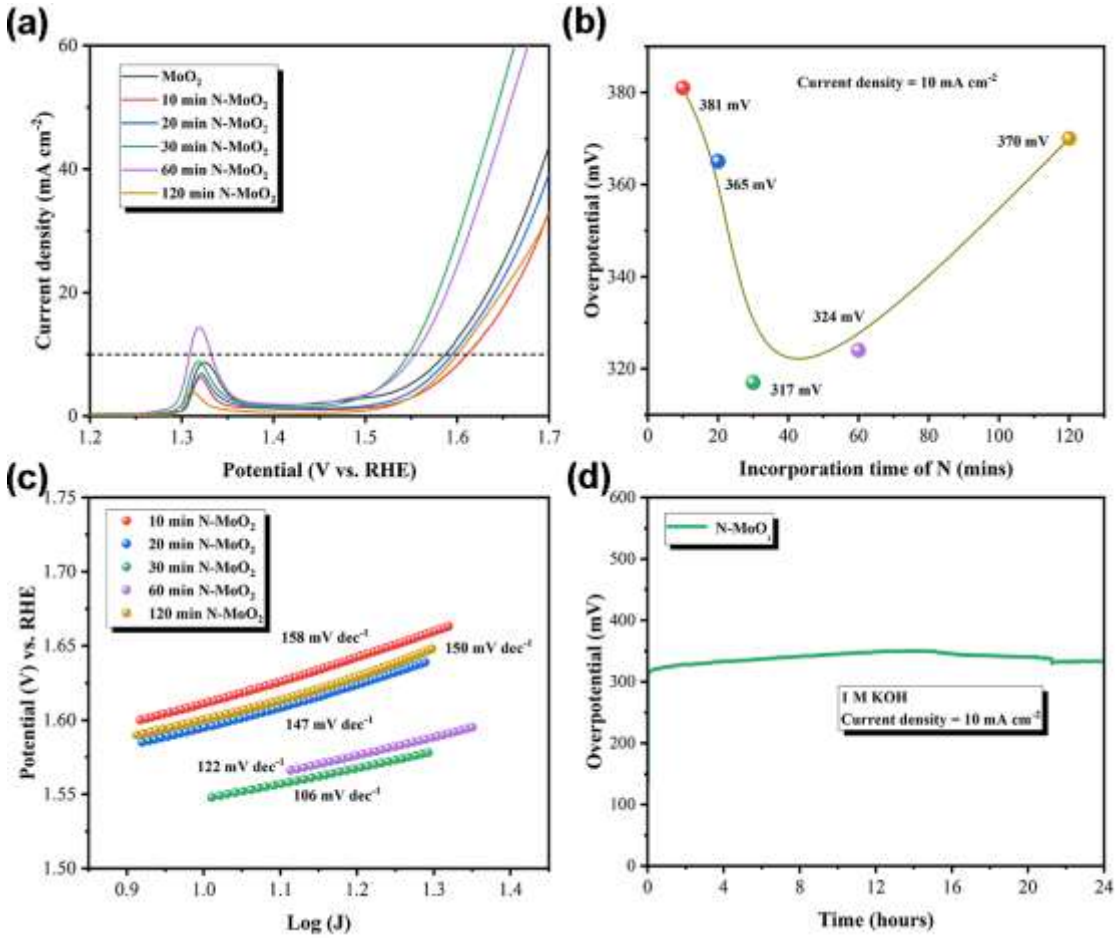

Fig. S10 (a) Polarization curves. (b) Overpotential comparison diagram at 10 mA cm^{-2}. (c) Tafel slopes of the as-prepared N-MoO_2 catalysts with different calcination times. (d) Chronopotentiometric responses of N-MoO_2 at the current density of 10 mA cm^{-2}.

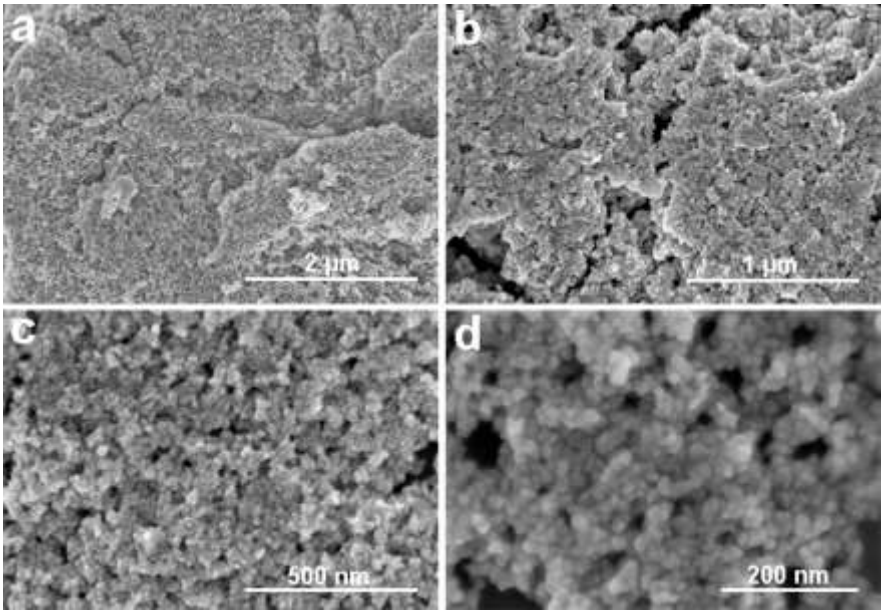

Fig. S11 SEM images of Ni/N-MoO_2.

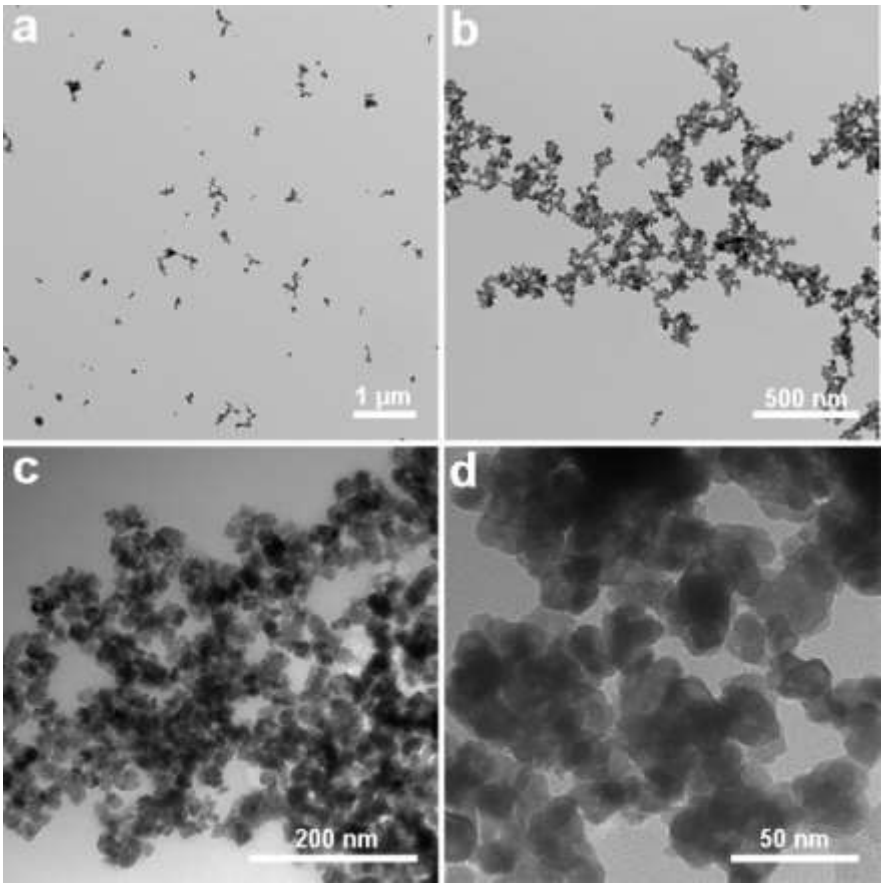

Fig. S12 TEM images of Ni/N-MoO_2.

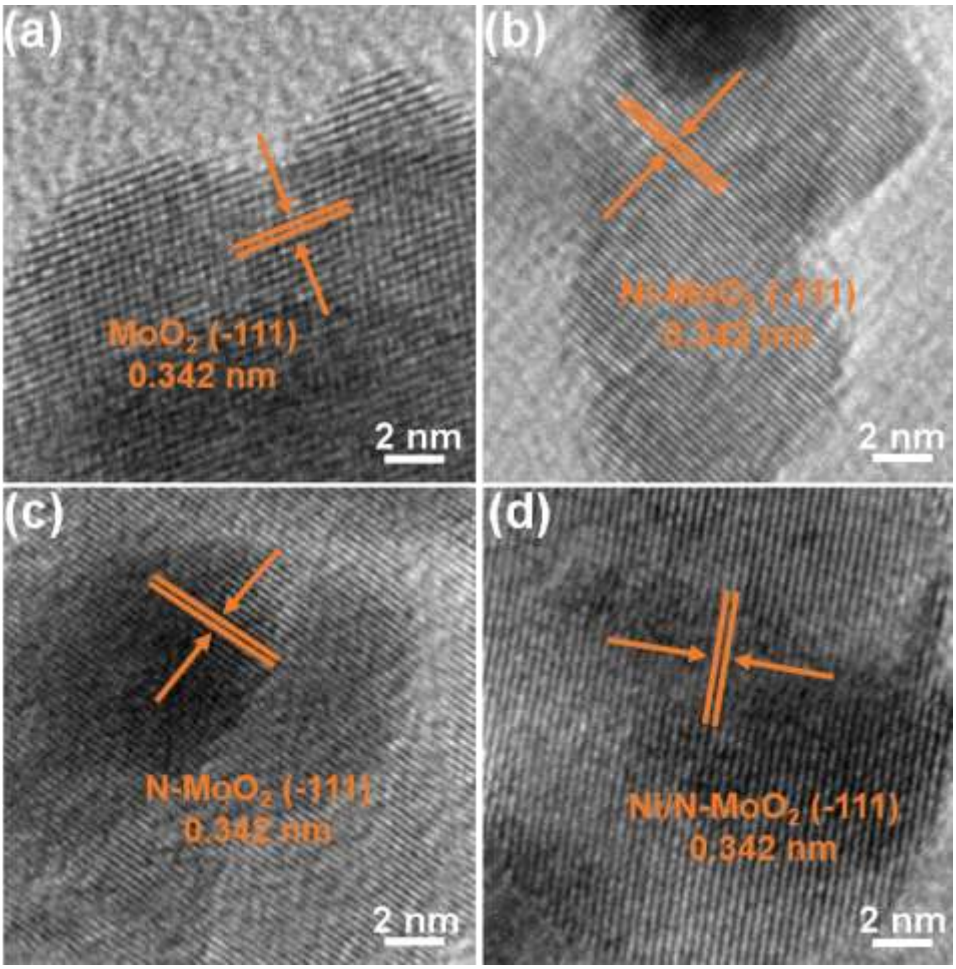

Fig. S13 HRTEM images of (a) MoO_2, (b) Ni-MoO_2, (c) N-MoO_2, and (d) Ni/N-MoO_2.

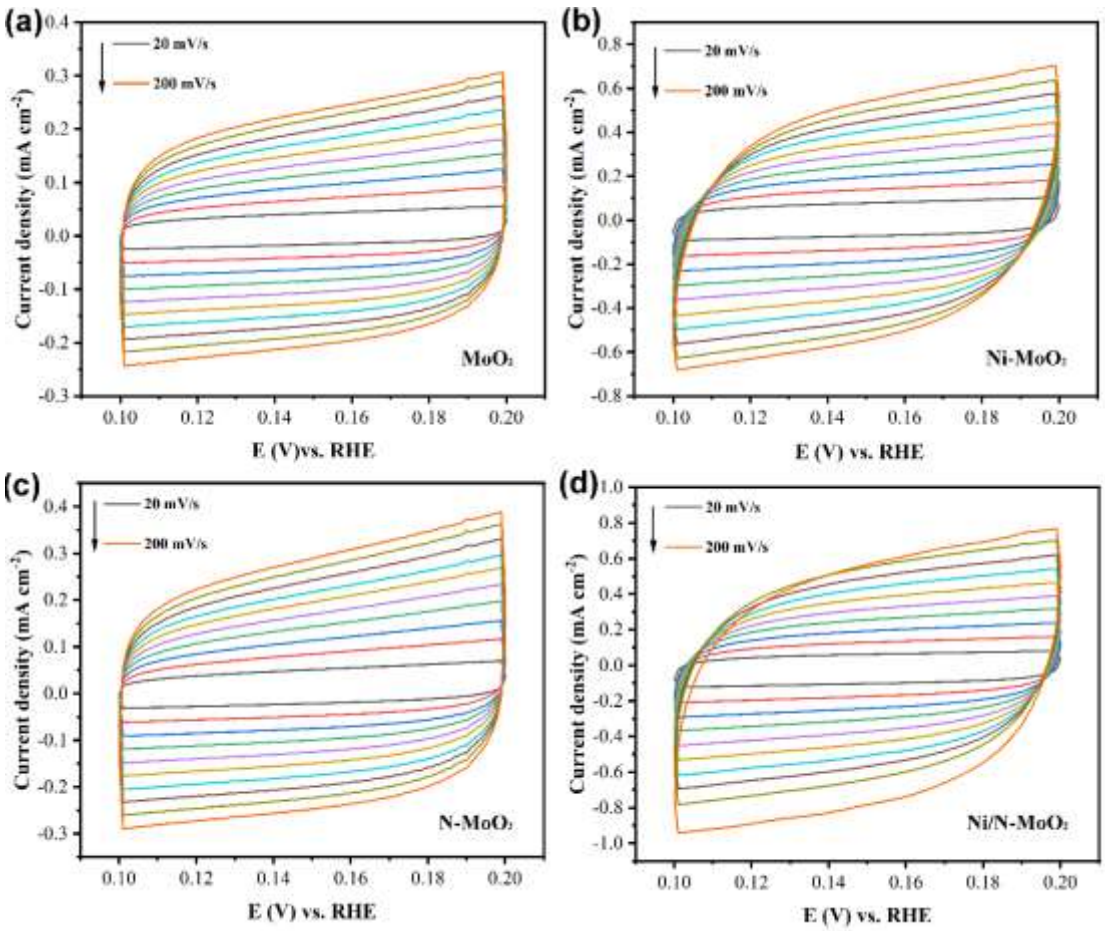

Fig. S14 The closed CV curves of the (a) MoO_2, (b) Ni-MoO_2, (c) N-MoO_2, and (d) Ni/N-MoO_2 catalysts.

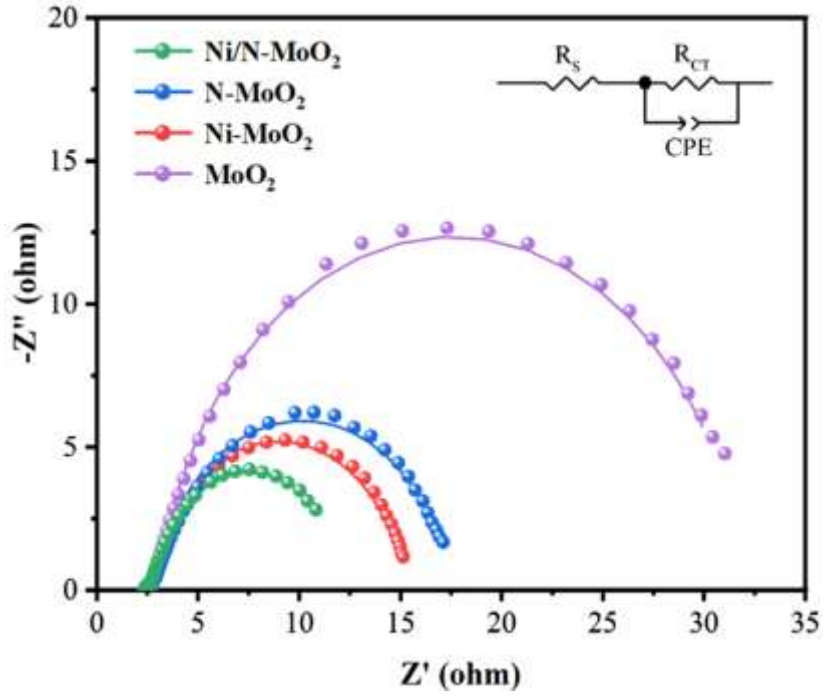

Fig. S15 Nyquist plots of EIS of the MoO_2, Ni-MoO_2, N-MoO_2, and Ni/N-MoO_2 catalysts.

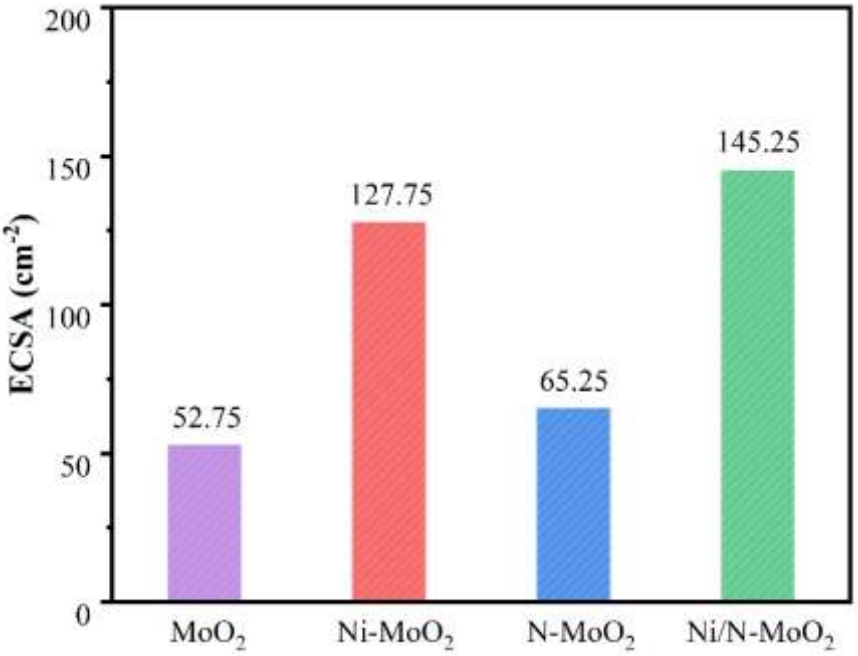

Fig. S16 ECSA of MoO_2, Ni-MoO_2, N-MoO_2 and Ni/N-MoO_2 in 1.0 M KOH.

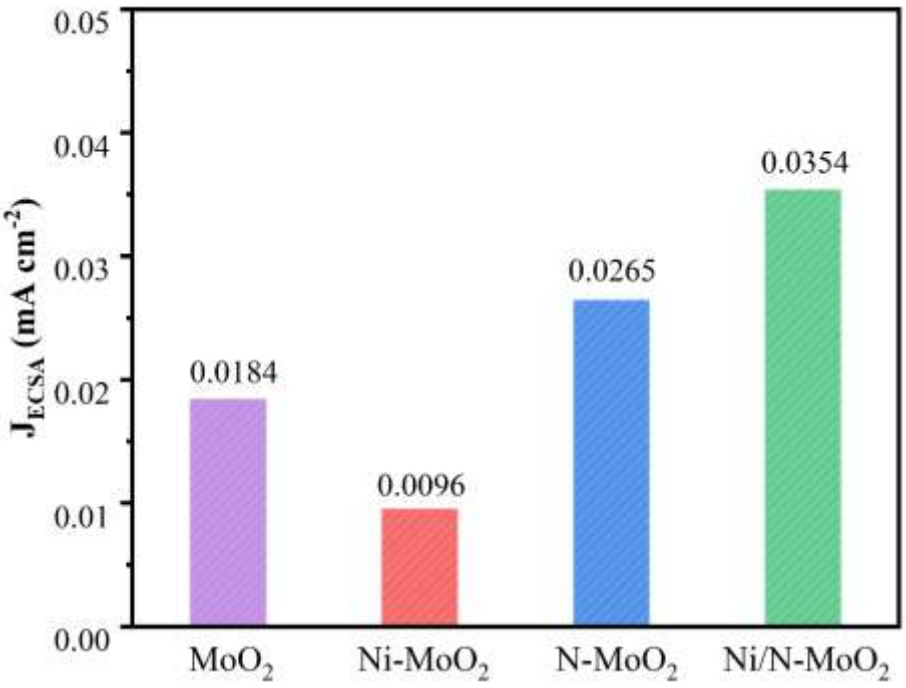

Fig. S17 The corresponding bar graph of the ECSA-normalized current density at the overpotential of 300 mV.

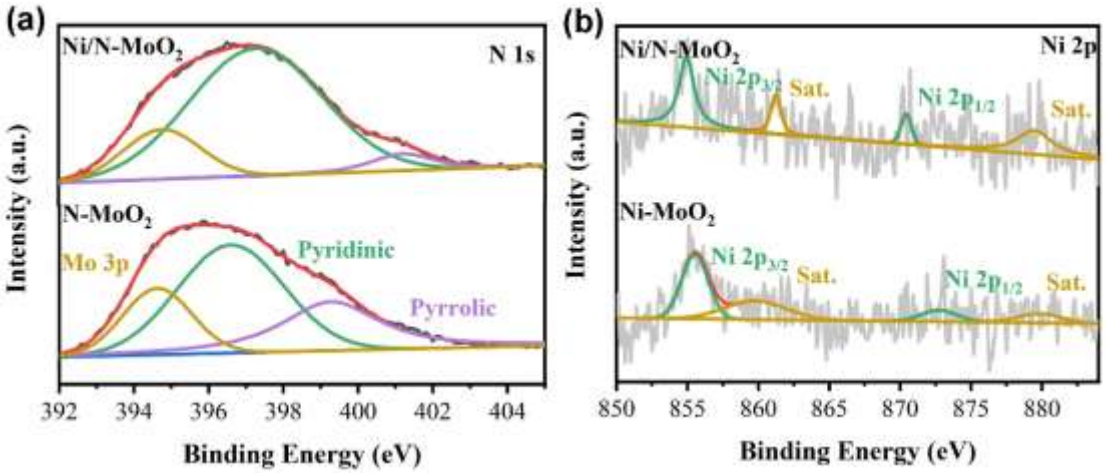

Fig. S18 XPS spectra of (a) N 1s orbital for N-MoO_2 and Ni/N-MoO_2. (b) Ni 2p orbital for Ni-MoO_2 and Ni/N-MoO_2.

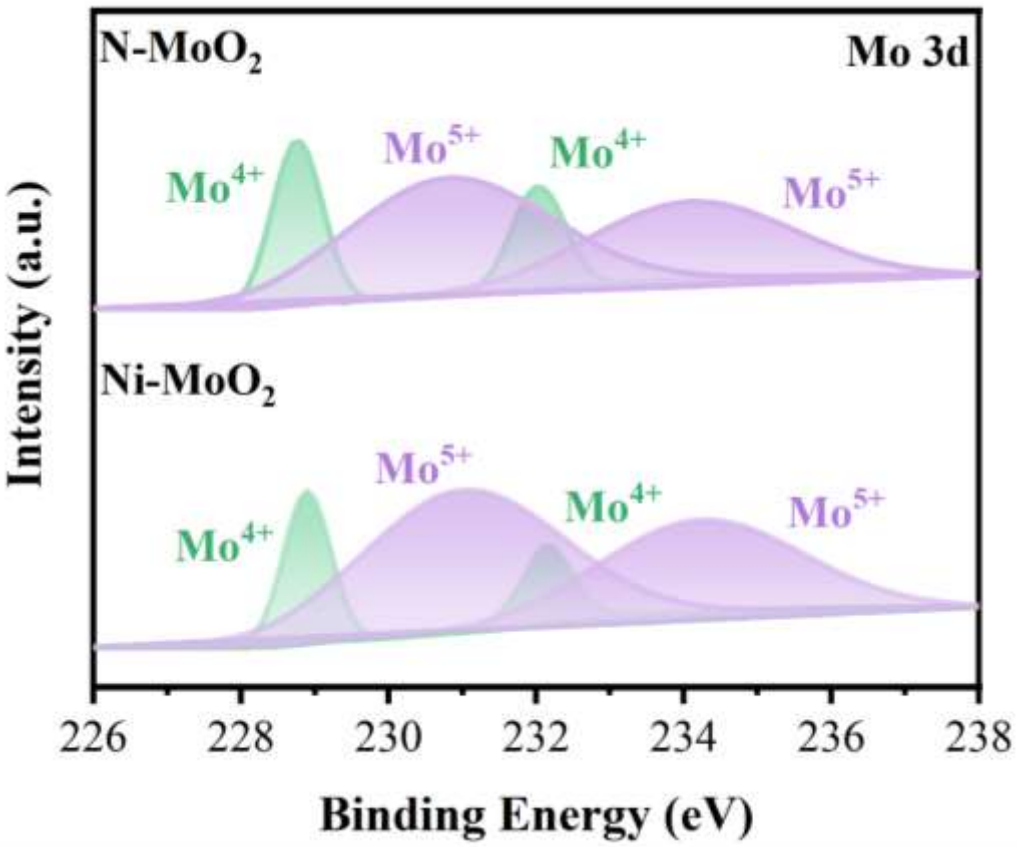

Fig. S19 Mo 3d XPS of Ni-MoO_2 and N-MoO_2.

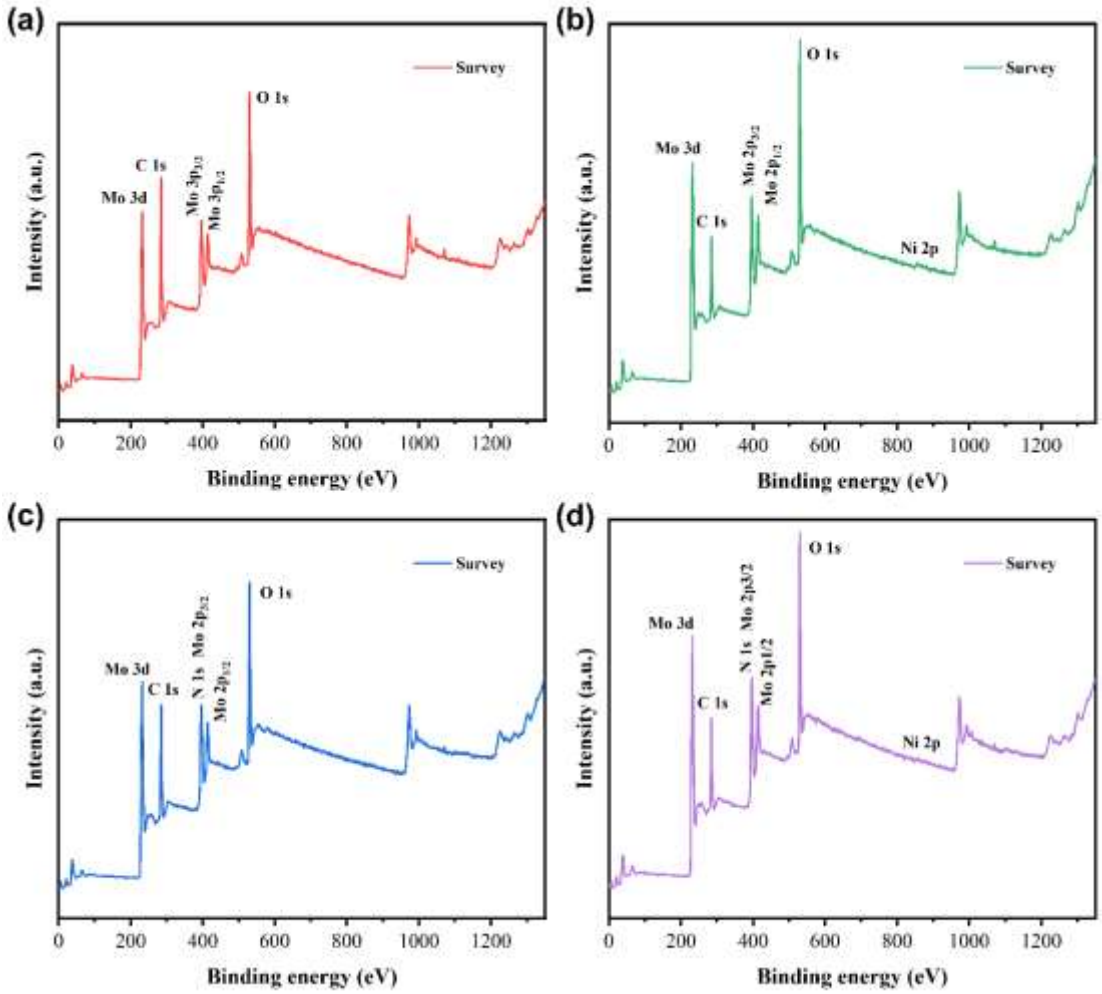

Fig. S20 XPS survey spectra of (a) MoO_2, (b) Ni-MoO_2, (c) N-MoO_2, and (d) Ni/N-MoO_2.

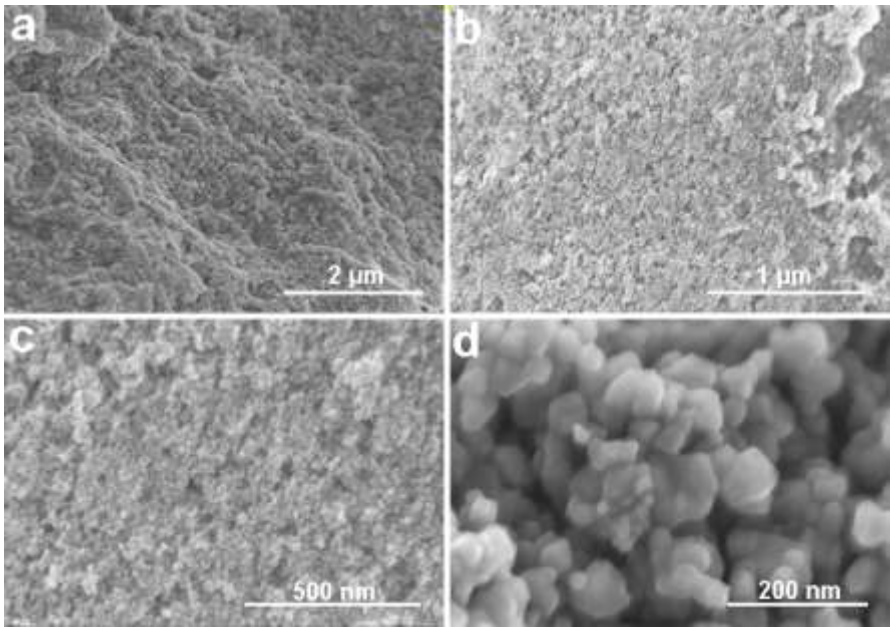

Fig. S21 SEM images of Ni/N-MoO_2 after OER process.

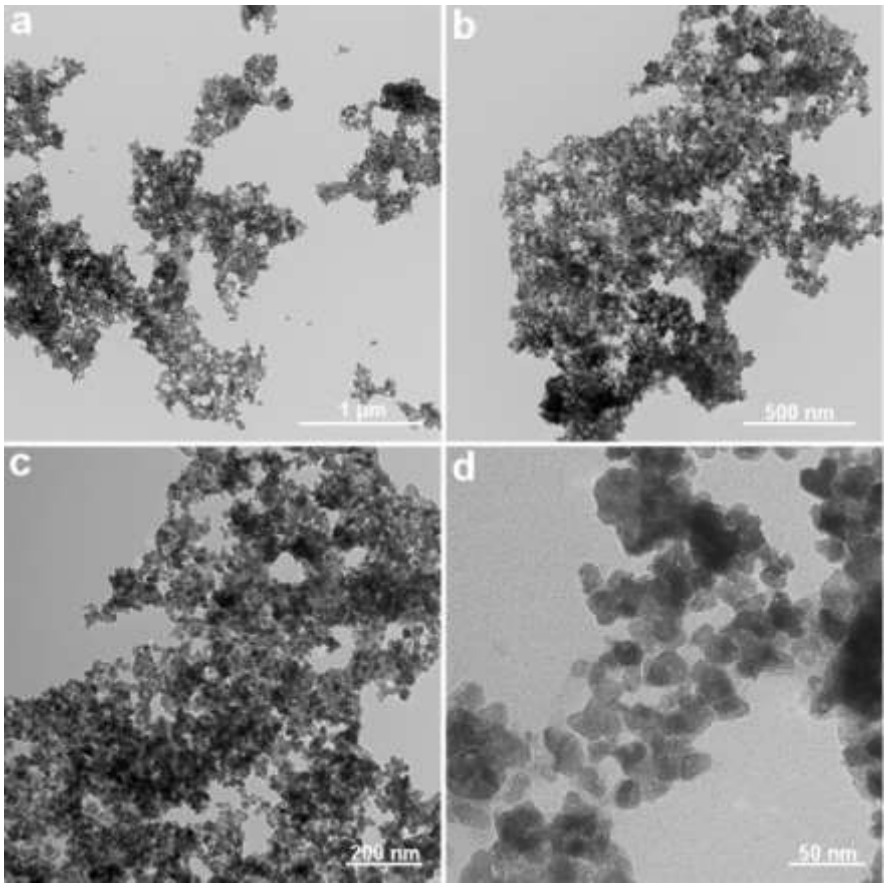

Fig. S22 TEM images of Ni/N-MoO_2 after the OER process.

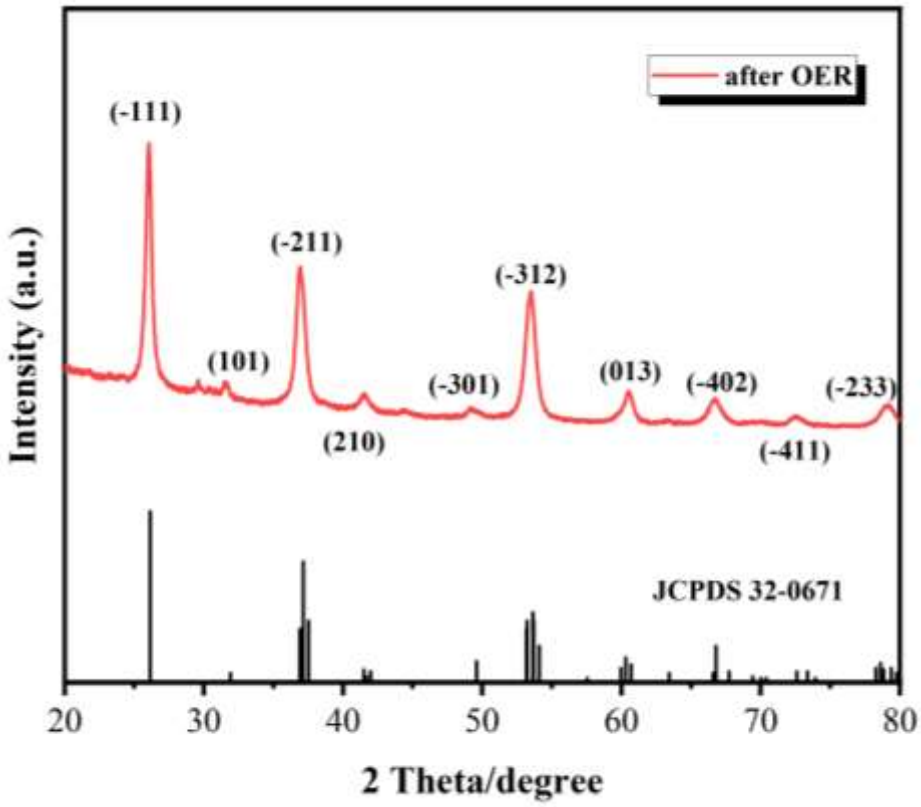

Fig. S23 XRD patterns of Ni/N-MoO_2 after the OER process.

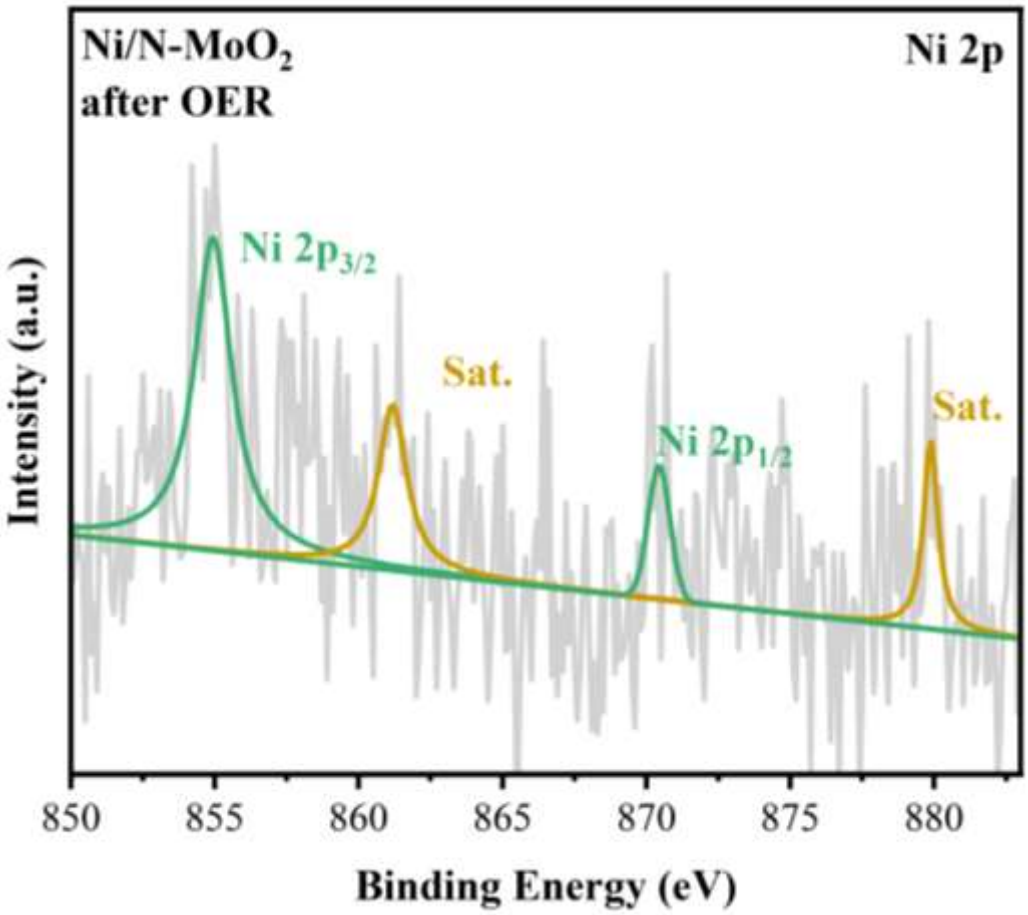

Fig. S24 The XPS spectrum of Ni 2p orbital after the OER process.

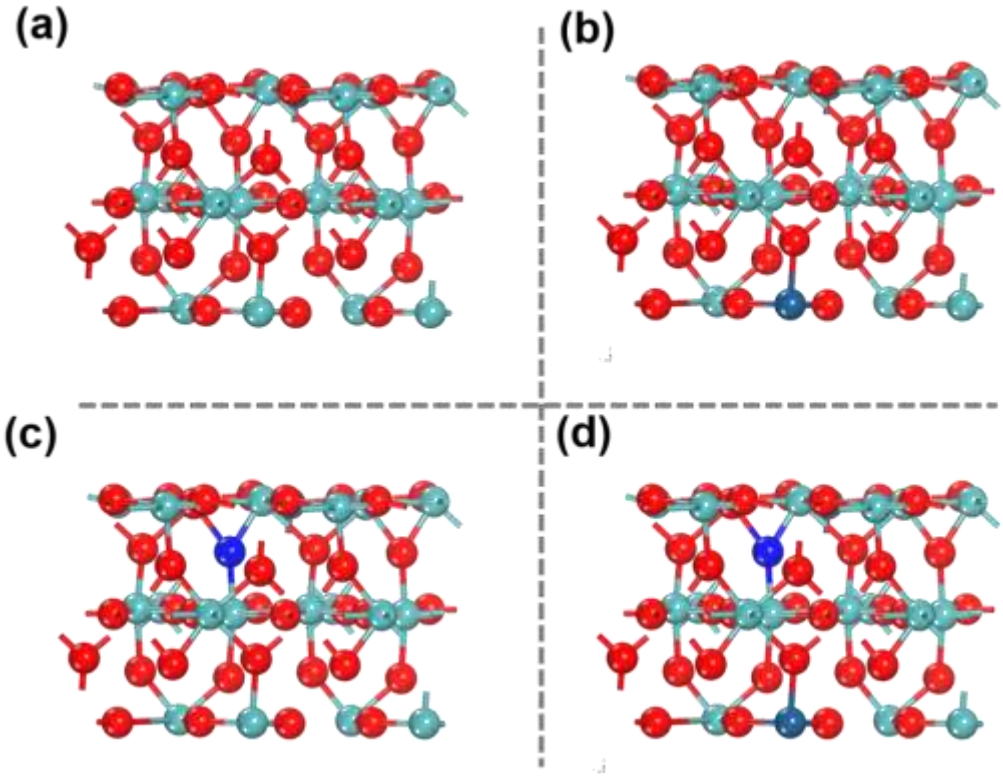

Fig. S25 Structure models of the (a) MoO_2, (b) Ni-MoO_2, (c) N-MoO_2 and (d) Ni/N-MoO_2.

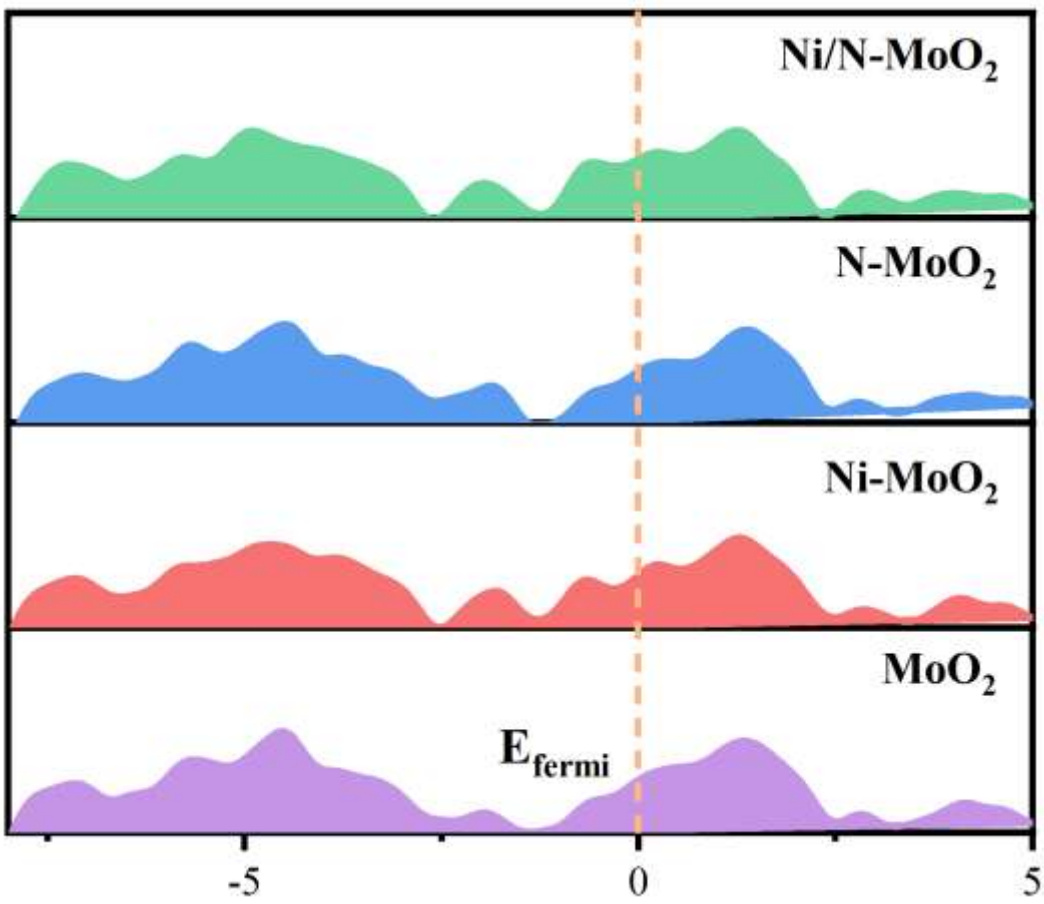

Fig. S26 Total density of states for MoO_2, Ni-MoO_2, N-MoO_2, Ni/N-MoO_2.

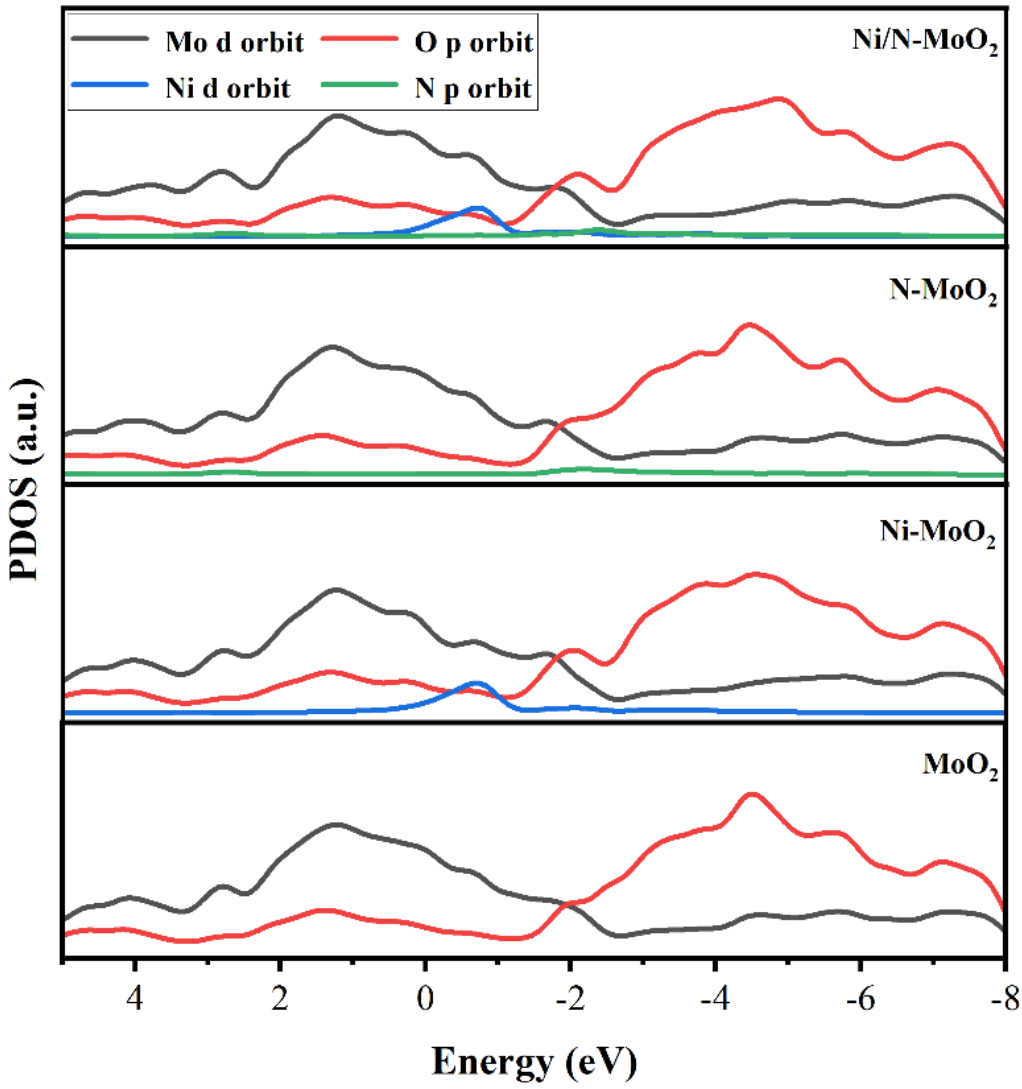

Fig. S27 Partial electronic density of states (PDOS) of the Mo d orbit, O p orbit, Ni d orbit, and N d orbit in the MoO_2, Ni-MoO_2, N-MoO_2, and Ni/N-MoO_2.

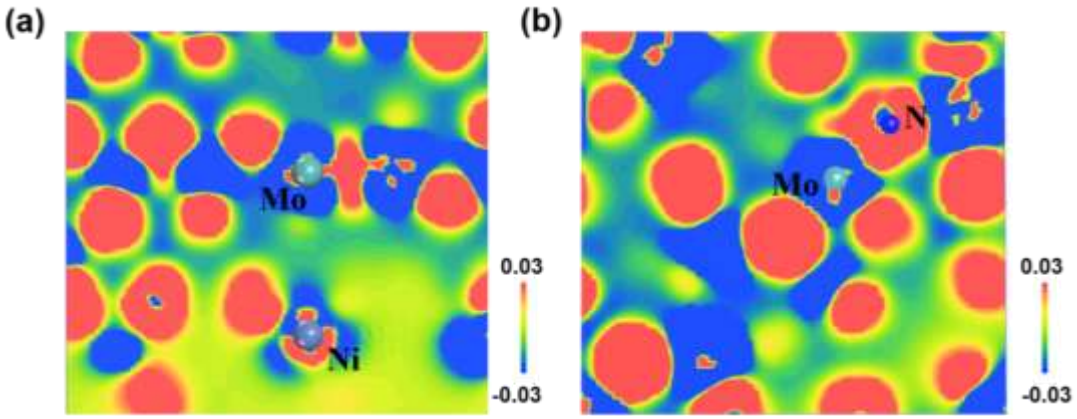

Fig. S28 The electron density differences of (a) Ni-MoO_2 and (b) N-MoO_2.

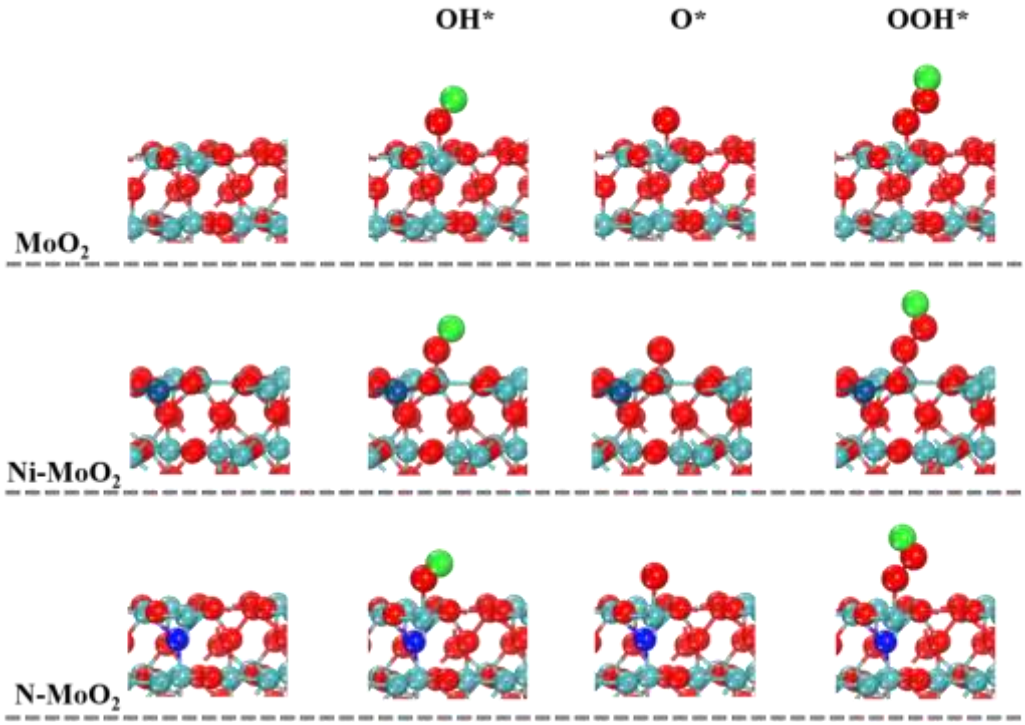

Fig. S29 The HER process and corresponding chemisorption models of MoO_2, Ni-MoO_2, and N-MoO_2.

Table 1. Summary of OER catalytic activities of representative MoO_2-based catalysts in alkaline electrolyte.

Catalysts	Electrolyte	η10 (mV)	Ref.
Ni/N-MoO_2	1.0 M KOH	270	This work
MoO_2@3DC	1.0 M KOH	348	[1]
MoO_2/NF	1.0 M KOH	340	[2]
MoO_2 nanosheet	1.0 M KOH	300	[3]
Ni/MoO_2	1.0 M KOH	287	[4]
MoO_2-$Co_2Mo_3O_8$	1.0 M KOH	320	[5]
CMO@NC	1.0 M KOH	272	[6]
MoO_2@NC	1.0 M KOH	302	[7]
MoO_{2-x}+OH^-	1.0 M KOH	296	[8]
CoO-MoO_2	1.0 M KOH	312	[9]
MoO_2/$CoC_2O_4 \cdot 2H_2O$	1.0 M KOH	330	[10]
MoO_2@MoS_2@Co_9S_8	1.0 M KOH	310	[11]
Ni-MoO_2@SCG	1.0 M KOH	278	[12]
$NiMoO_{4-x}$/MoO_2	1.0 M KOH	233	[13]
Fe_2O_3/NiO/MoO_2	1.0 M KOH	282	[14]
MCF/NPCCNT	1.0 M KOH	292	[15]
MoO_2-$Co_2Mo_3O_8$@C	1.0 M KOH	320	[16]
Co/MoO_2	1.0 M KOH	318	[17]
MoO_2/$Ni_{0.2}Mo_{0.8}N$	1.0 M KOH	264	[18]
MoO_2@MoS_2@Co_9S_8	1.0 M KOH	310	[19]
Ni_3Mo_3N-MoO_2-NiO	1.0 M KOH	363	[20]

References

1. W. Zhu, X. H. Yan, X. P. Huang, S. T. Wu, H. Chen, J. M. Pan, T. Li and Z. Shahnavaz, *Ceram. Int.* 2023, **49**, 5646-5656.
2. H. Y. Wang, J. T. Ren, C. C. Weng, X. W. Lv and Z. Y. Yuan, *Chem. Eng. J.* 2021, **426**, 130761.
3. Y. S. Jin, H. T. Wang, J. J. Li, X. Yue, Y. J. Han, P. K. Shen and Y. Cui, *Adv. Mater*. 2016, **28**, 3785-3790.
4. S. Ni, H. N. Qu, H. F. Xing, Z. H. Xu, X. Y. Zhu, M. L. Yuan, L. Wang, J. M. Yu, Y. Q. Li, L. R. Yang and H. Z. Liu, *ACS Appl. Mater. Interfaces*, 2021, **13**, 17501-17510.
5. Y. Q. Li, H. B. Xu, H. Y. Huang, C. Wang, L. G. Gao and T. L, Ma, *Chem. Commun*. 2018, **54**, 2739-2742.
6. W. Yaseen, M. Xie, B. A. Yusuf, Y. G. Xu, M. Rafiq, N. Ullah, P. Y. Zhou, X. Li and J. M. Xie, *Int. J. Hydrogen Energ.* 2022, **47**, 15673-15686.
7. M. L. Mei, X. X. Xu, Y. Wang, X. J Wang and Y. Q. Huo, *J. Name*. 2013, **00**, 1-3.
8. P. Guha, B. Mohanty, R. Thapa, R. M. Kadam, P. V. Satyam and B. K. Jena, *ACS Appl. Energy Mater*. 2020, **3**, 5208-5218.
9. F. L. Lyu, Y. C. Bai, Z. W. Li, W. J. Xu, Q. F. Wang, J. Mao, L. Wang, X. W. Zhang, and Y. D. Yin, *Adv. Funct. Mater*. 2017, **27**, 1702324.
10. S. Ghosh, H. R. Inta, S. Ganguli, G. Tudu, H. V. S. R. M. Koppisetti and V. Mahalingam, *J. Phys. Chem. C*. 2020, **124**, 20010-20020.

11. Y. Q. Li, C. Wang, M. Cui, J. B. Xiong, L. W. Mi, S. Chen, *Appl. Surf. Sci*. 2021, **543**, 148804.

12. T. Zhou, Y. Q. Huang, A. Ali, P. K. Shen, *J. Electroanal. Chem*. 2021, **897**, 115555.

13. Z. Zhang, X. X. Ma, and J. L. Tang, *J. Mater. Chem. A*. 2018, **6**, 12361-12369.

14. X. J. Zhang, Y. F. Chen, M. L. Chen, B. Wang, B. Yu, X. Q. Wang, W. L. Zhang, D. G. Yang, *Nanoscale*, 2020, **12**, 3777-3786.

15. X. J. Zhang, Y. F. Chen, M. L. Chen, B. Yu, B. Wang, X. Q. Wang, W. L. Zhang, D. X. Yang, J. Colloid. *Interf. Sci*, 2021, **581**, 608-618.

16. Y. Q. Li, H. B. Xu, H. Y. Huang, C. Wang, L. G. Gao, T. L. Ma, *Chem. Commun*, 2018, **54**, 2739-2742.

17. L. Xia, Y. J. Li, H. Song, X. X. Li, W. J. Gong, X. Y. Jiang, M. Javanbakht, X. M. Zhang, B. Gao, P. K. Chu, *Rsc. Adv*, 2022, **12**, 34760-34765.

18. Y. W. Hu, H. Yang, J. Chen, *New. J. Chem*, 2023, **47**, 10916-10920.

19. Y. Q. Li, C. Wang, M. Cui, J. B. Xiong, L. W. Mi, S. R. Chen, *Appl. Surf. Sci*, 2021, **543**, 148804.

20. B. Peng, J. Hao, Z. M. Tian, Q. C. Xu, C. X. Ma, G. Y. Liu, Y. Y. Shi, W. J. Zheng, *Energ. Fuel*, 2022, **36**, 4902-4910